Insights into the interaction between UGGT, the gatekeeper of folding in the ER, and its partner, the selenoprotein SEP15

PNAS RESEARCH ARTICLE | BIOPHYSICS AND COMPUTATIONAL BIOLOGY OPEN ACCESS

Insights into the interaction between UGGT, the gatekeeper of folding in the ER, and its partner, the selenoprotein SEP15

Robert V. Williams[a], Kevin P. Guay[a,b], Owen A. Hurlbut Lesk[a], Eugenia M. Clerico[a], Daniel N. Hebert[a,b,1], and Lila M. Gierasch[a,b,c,1]

Edited by Ulrich Hartl, Max-Planck-Institut fur Biochemie, Martinsried, Germany; received October 5, 2023; accepted February 4, 2024

The enzyme UDP-glucose: glycoprotein glucosyltransferase (UGGT) is the gatekeeper of protein folding within the endoplasmic reticulum (ER). One-third of the human proteome traverses the ER where folding and maturation are facilitated by a complex protein homeostasis network. Both glycan modifications and disulfide bonds are of key importance in the maturation of these ER proteins. The actions of UGGT are intimately linked to the glycan code for folding and maturation of secretory proteins in the ER. UGGT selectively glucosylates the N-linked glycan of misfolded proteins so that they can reenter the lectin-folding chaperone cycle and be retained within the ER for further attempts at folding. An intriguing aspect of UGGT function is its interaction with its poorly understood cochaperone, the 15 kDa selenoprotein known as SELENOF or SEP15. This small protein contains a rare selenocysteine residue proposed to act as an oxidoreductase toward UGGT substrates. AlphaFold2 predictions of the UGGT1/SEP15 complex provide insight into this complex at a structural level. The predicted UGGT1/SEP15 interaction interface was validated by mutagenesis and coimmunoprecipitation experiments. These results serve as a springboard for models of the integrated action of UGGT1 and SEP15.

UGGT | SEP15 | endoplasmic reticulum | protein folding

Significance

One-third of the human proteome matures within the endoplasmic reticulum (ER) where these proteins are modified with N-linked glycans. These carbohydrate modifications play an important role in the folding pathway of secretory proteins, and a key player in surveillance of their folding is the enzyme UDP-glucose: glycoprotein glucosyltransferase (UGGT). UGGT forms a complex with a redox-active cochaperone, the 15 kDa selenoprotein (SEP15). We use the machine learning program AlphaFold2 to predict the structure of the UGGT1/SEP15 complex and validate the prediction. The results provide insight into the potential functions of this complex and the mechanism whereby they oversee ER protein folding.

Proper folding of proteins is critical for their biological function. In addition to their loss of function, misfolded proteins are prone to aggregation, which can result in the onset of disease. To mitigate these problems, cells have evolved a variety of sophisticated biochemical processes that support the proper folding of the proteome. In humans, one-third of the proteome contains a signal sequence for targeting to the secretory pathway (1), which begins with entry into the endoplasmic reticulum (ER). About 80% of secretory proteins are modified with N-linked glycans (2). Carbohydrates play a key role in the productive folding and maturation of glycosylated proteins through the lectin chaperone cycle (Fig. 1) (3, 4).

The lectin chaperone cycle begins with the cotranslational addition of glycans to asparagine residues within N-X-S/T/C consensus sequences (sequons) (5) by oligosaccharyltransferase A (OST-A). This enzyme catalyzes the en bloc transfer of a $Glc_3Man_9GlcNAc_2$ carbohydrate from a lipid-linked precursor to the glycosylation site (Fig. 1, step 1). The glycan is then rapidly trimmed by α-glucosidases I and II (GlsI, GlsII) to a monoglucosylated form (Fig. 1, step 2), which can be recognized by the lectin chaperones calnexin (CNX) and calreticulin (CRT, Fig. 1, step 3). CNX and CRT serve as scaffolds for other cochaperones to bind, including protein disulfide-isomerase A3 (ERp57), ER-resident protein 29 (ERp29), and peptidyl-prolyl cis-trans isomerase B (CypB), all of which aid in proper protein folding (6). When the protein substrate dissociates from the lectin chaperones, GlsII acts again to remove the terminal glucose residue (Fig. 1, step 4). At this point, the protein can continue to fold to its native form or, if requiring further folding assistance, it may be recognized by the key quality control enzyme UDP-glucose: glycoprotein glucosyltransferase (UGGT, Fig. 1, step 5). Using an unknown mechanism of recognition, UGGT senses the folding state of the glycoprotein and selectively reglucosylates specific glycans. This process regenerates monoglucosylated species, enabling their reentry into the lectin chaperone cycle for additional rounds of lectin chaperone-assisted folding (Fig. 1, step 3).

The biophysical mechanism underlying the gatekeeping activity of UGGT has received considerable attention. Key experiments have shown that UGGT selectively glucosylates model glycoprotein substrates exhibiting molten globule structural characteristics (7). Additional studies have shown that UGGT reglucosylates sites close to areas of structural perturbation (8, 9). More recently, X-ray crystal structures of UGGT homologs from thermophilic yeast have suggested that interdomain motion is important for UGGT function (10, 11).

Author affiliations: [a]Department of Biochemistry and Molecular Biology, University of Massachusetts, Amherst, MA 01003; [b]Graduate Program in Molecular and Cellular Biology, University of Massachusetts, Amherst, MA 01003; and [c]Department of Chemistry, University of Massachusetts, Amherst, MA 01003

Author contributions: R.V.W., K.P.G., O.A.H.L., E.M.C., D.N.H., and L.M.G. designed research; R.V.W., K.P.G., and O.A.H.L. performed research; K.P.G. contributed new reagents/analytic tools; R.V.W., K.P.G., O.A.H.L., E.M.C., D.N.H., and L.M.G. analyzed data; and R.V.W., K.P.G., O.A.H.L., E.M.C., D.N.H., and L.M.G. wrote the paper.

The authors declare no competing interest.

This article is a PNAS Direct Submission.

[1]To whom correspondence may be addressed. Email: dhebert@biochem.umass.edu or gierasch@biochem.umass.edu.

This article contains supporting information online at https://www.pnas.org/lookup/suppl/doi:10.1073/pnas.2315009121/-/DCSupplemental.

Published August 12, 2024.

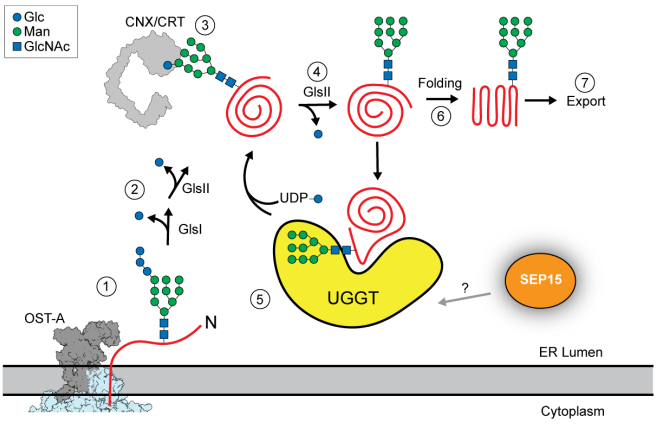

Fig. 1. Glycoprotein maturation is overseen by a dedicated quality control system in the ER. 1) Oligosaccharyltransferase A (OST-A) scans a nascent polypeptide and glycosylates asparagine residues within N-X-S/T/C amino acid motifs. 2) The two terminal glucose residues of the glycan moiety are rapidly trimmed by glucosidases I and II (GlsI and GlsII). 3) The resulting monoglucosylated glycan serves as a binding site for the lectin chaperones, calnexin (CNX) and calreticulin (CRT), which promote protein folding. 4) Upon removal of the final glucose residue by GlsII the client is released. 5) If the released glycoprotein has not achieved its native fold, it is bound by UGGT, which senses the folding status of the glycoprotein and selectively reglucosylates the N-glycan. 6) The glycoprotein released from the lectin chaperones CNX/CRT and cochaperones, either in the first time through the cycle or after reentering the cycle if reglucosylated by UGGT, may achieve its native fold and proceed to exit the ER for export via ER exit sites (7). A significant fraction of the UGGT in the ER is in complex with the SEP15, but the function of this selenoprotein is unknown.

A significant fraction of the UGGT in the ER is in a stable complex with a poorly understood cochaperone, the 15 kDa selenoprotein (SEP15 with its human gene named *SELENOF*). The role of SEP15 in the partnership with UGGT is a mystery. In mammalian cells, all SEP15 was found in complex with UGGT, whereas not all UGGT was associated with SEP15 (12). While SEP15 lacks a typical ER retrieval motif (e.g., KDEL), it is nonetheless retained in the ER, presumably through its tight association with UGGT. Several lines of evidence indicate that SEP15 may play an important role in ER protein quality control. First, like many other proteins that participate in the ER quality control network, expression of SEP15 was altered during the unfolded protein response (UPR) (13). Next, a *Selenof*$^{-/-}$ mouse developed cataracts at an early age and showed signs of oxidative stress in the liver (14). Finally, *Selenof* knockout mouse B cells secrete higher levels of IgM, but most of this product is not functional (15). These findings led to the proposal that SEP15 facilitates the folding and maturation of a subset of secretory proteins, especially those rich in disulfide bonds (15).

Despite its apparent importance in maturation of secretory proteins, the mechanism of action of SEP15 is poorly understood. This small protein contains a single selenocysteine (Sec, U) residue, a cysteine analog where the sulfur atom has been replaced with selenium (16). Only 25 selenoproteins are found in humans (16). The unusual properties of the selenocysteine residue are presumably exploited in the functions of SEP15 in ER quality control: The selenol moiety of Sec has a pK_a of 5.2, much lower than the pK_a for Cys thiols (8.3), and serves as a better nucleophile (17). Based on the reported reduction potential of –222 mV, SEP15 may act as either a disulfide reductase or an isomerase (18).

A better understanding of SEP15 function is limited by the lack of structural data, both on SEP15 itself and on its complex with UGGT. SEP15 is composed of two domains: a C-terminal thioredoxin-like (TRXL) domain and an N-terminal Cys-rich domain (CRD). The thioredoxin-like domain contains the single Sec residue as part of a redox-active C-G-U motif. An NMR solution structure of the TRXL domain of SEP15 from *Drosophila melanogaster* has been reported and showed that the redox-active motif was exposed to solvent (18). Importantly, the CRD of SEP15 was shown via coimmunoprecipitation (co-IP) experiments with UGGT to be responsible in large measure for UGGT/SEP15 binding, but no structural data are available for this domain. An approximately 40-residue region of *D. melanogaster* UGGT was protected from hydrogen–deuterium exchange (HDX) in the presence of SEP15, suggesting that this region may be implicated in SEP15 binding (19). However, there is no structure for the complex of UGGT with SEP15 that may help to reveal how its function may be modulated by the selenoprotein.

Here, we leverage the recent advances in structural prediction enabled by AlphaFold2 to provide insight into the nature of the UGGT1/SEP15 interaction (20, 21). We generated a structural prediction of the human UGGT1/SEP15 complex, assessed its consistency with reported data about the complex, and experimentally validated the predicted protein–protein interface. Using the prediction as a guide, we propose potential mechanisms for the action of UGGT1/SEP15 on glycoprotein substrates.

Results

AlphaFold2 Predicts a Small Helical Domain to Be the SEP15-Binding Region of Human UGGT1. The structure of human UGGT has not been determined, but several crystal structures have been solved for UGGT homologs from thermophilic yeast (10, 11, 22). These structures are highly informative in that they reveal a complex topological organization of the major domains of UGGTs: The domains are indicated in the diagram of the human UGGT sequence in Fig. 1*A*, which shows that in addition to the four thioredoxin-like domains (TRXL1-4) [Note: TRXL domains are not precisely defined but contain a mixed α/β structure similar to thioredoxin], the two β-sheet domains (βS1 and 2), and the glucosyltransferase domain (GT) present in the yeast UGGTs, there is an additional small domain between βS1 and the first portion of TRXL1. Because this region is absent in the thermophilic yeast, their structures do not shed light on its structure. Importantly, this element of the human UGGT1 sequence contains the sequence from *D. melanogaster* UGGT that was previously implicated in binding Sep15 by HDX mass spectrometry (19). We hypothesize that this domain is indeed the SEP15-binding region (SBR). To gain structural insight into its potential as a SEP15 binding site, we predicted the structure of human UGGT1 using AlphaFold2 (20). The resulting predicted structure is similar to all previously solved crystal structures of UGGT homologs (10, 11, 22), but with one key difference: AlphaFold2 predicts that the putative SEP15 binding domain adopts two α-helices with a loop between and a packing interface between them (Fig. 2*B*). Provocatively, the putative SBR of UGGT1 has a continuous hydrophobic patch that we speculate may mediate the interaction with SEP15 (Fig. 2*C*).

To test the role of the helix–loop–helix proposed as an SBR, we generated a sequence alignment of UGGT homologs ranging from humans to yeast (Fig. 2*D*). A clear difference is observed between UGGT homologs from organisms that lack SEP15 and those that have SEP15 homologs. The former display large gaps in the sequence alignment in the proposed SBR. The differences in primary sequence are fully consistent with the results of the HDX study (19) and taken together support the hypothesis that this region mediates the interaction with SEP15.

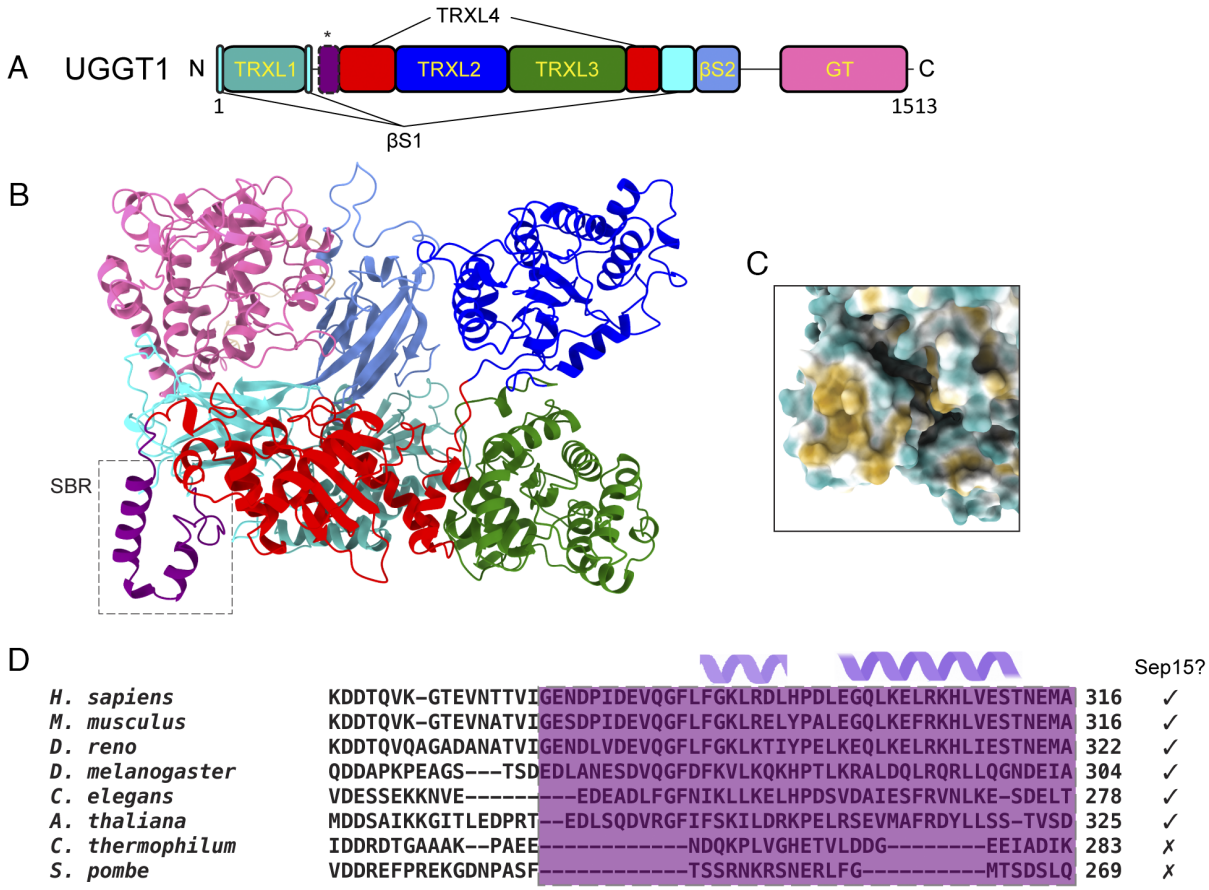

Fig. 2. AlphaFold2 predicts a potential SEP15-binding domain in human UGGT1. (*A*) Cartoon of the human UGGT1 sequence. UGGT1 has a complex topology of eight domains: four thioredoxin-like domains (TRXL1 to 4), two β-sheet domains (β*S*1 and β*S*2), a glucosyltransferase domain (GT), and a domain absent in the fungal UGGTs (*). Note that TRXL4 and βS1 are composed of noncontiguous regions of the primary sequence. (*B*) AlphaFold2 prediction of the structure of human UGGT1. Domains are colored as in panel (*A*). The helix–loop–helix domain absent in previous crystal structures of UGGTs from thermophilic organisms lacking SEP15, which we propose to be the SEP15-binding region (SBR), is indicated by a dashed box. (*C*) A closer view of the SBR from (*B*), shown as a molecular lipophilicity potential surface created using ChimeraX (23). A hydrophobic patch (gold) in this region is a likely candidate for interacting with SEP15. (*D*) A multiple sequence alignment of eukaryotic UGGTs shows significant differences. The UGGTs from organisms that lack an SEP15 homolog have gaps in the region corresponding to the helix–loop–helix predicted in human UGGT1. Moreover, the region identified as a SEP15 binding region is shown by the purple box. (Note: For those organisms with multiple UGGT paralogs, only the UGGT1 sequence is shown). The α-helices observed in the predicted structure are indicated above the sequences.

An additional striking feature of the UGGT1 prediction is the large cleft running through the center of the protein. One wall of this "canyon" is formed by the GT and βS2 domains, while the TRXL2 domain forms the other wall. This feature was previously observed in the crystal structures of UGGT homologs and is thought to play a key role in UGGT-substrate interactions (11).

Protein sequence conservation is often strongest for functionally important residues. Using ConSurf (24), we mapped sequence conservation of UGGTs from species with a SEP15 homolog onto the AlphaFold2 prediction of human UGGT1 (*SI Appendix*, Fig. S2). The strongest conservation is observed for the GT domain. Additional patches of conserved residues are observed in the SBR. Several of the residues forming the hydrophobic patch (Fig. 2*C*) are also highly conserved, lending further support to the hypothesis that this site interacts with SEP15.

The Cysteine-Rich Domain of SEP15 Is Predicted to Be an α-Helical Domain. A combination of sequence information and biochemical experiments led to the conclusion that SEP15 is made up of two domains: a cysteine-rich domain (CRD) and a TRXL domain (Fig. 3*A*) (25). While a structure has been reported for the TRXL domain of SEP15, there are no experimental structures of the CRD of SEP15, which contributes the lion's share of the binding affinity of SEP15 for UGGT (25). We therefore predicted the structure of full-length human SEP15 using AlphaFold2. In agreement with previous reports, the predicted structure forms two domains separated by a short linker (Fig. 3*B*). The TRXL domain aligns well with the previously determined NMR solution structure of this domain from *D. melanogaster* Sep15 (*dm*Sep15) (*SI Appendix*, Fig. S2). Both structures show the same mixed α/β structure with the redox-active residue (Sec for human SEP15, but Cys for *dm*Sep15) exposed to solvent. Confidence in the prediction for this domain is very high, as measured by the predicted linear distance-difference test (pLDDT) reported by AlphaFold2. This per-residue metric ranges from 0 to 100, with higher scores indicating higher confidence. Scores above 90 have been shown to correspond to structures that accurately predict both protein backbone and side-chain orientation (26). The TRXL domain has an average pLDDT of 94 (*SI Appendix*, Fig. S3). The eight-residue linker between CRD and TRXL displays pLDDT scores from 57 to 81 indicating lower confidence for this region, most likely from its dynamic character.

The AlphaFold2-predicted structure of the CRD shows a predominantly helical fold, with three α-helices stabilized by three disulfide bridges between C10-C42, C21-C43, and C24-C39 (Fig. 3*C*). Interestingly, this set of disulfide bridges is not consistent with an earlier report that found disulfide bonds between

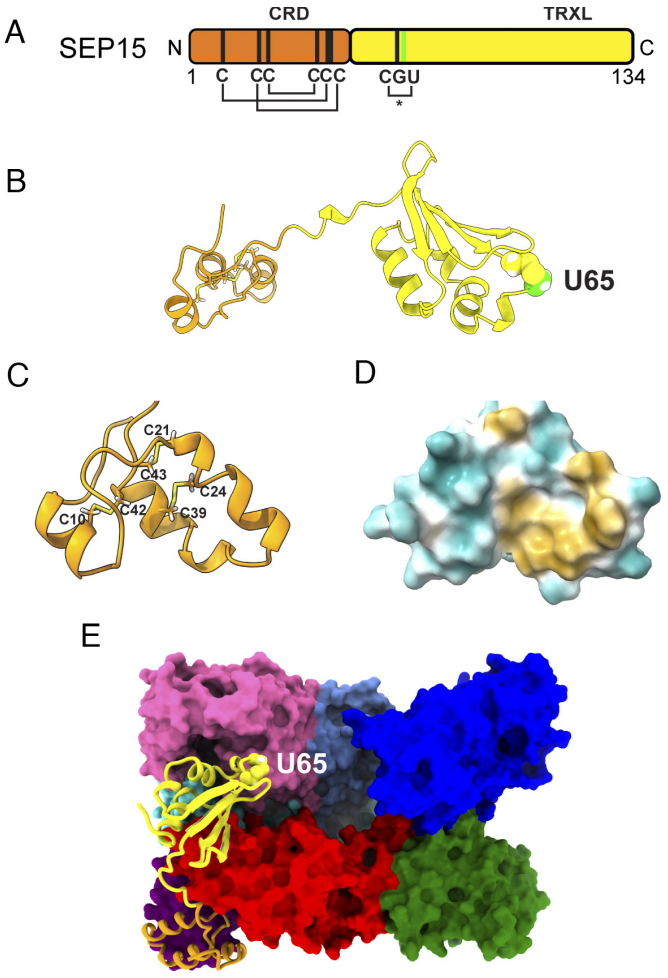

Fig. 3. AlphaFold2 prediction of SEP15 and the UGGT1/SEP15 complex. (*A*) SEP15 is composed of two domains: a cysteine-rich domain (CRD) and a thioredoxin-like domain (TRXL). The single selenocysteine (Sec, U) residue is found within the TRXL domain. The position of all Cys residues is indicated in black, and the Sec residue is indicated in bright green. The predicted disulfide pairings are shown. AlphaFold2 predicts a selenyl-sulfide pairing with the TRXL domain, but this reactive motif likely interconverts with a reduced form (indicated by an asterisk). (*B*) AlphaFold2 predicts a two-domain structure for SEP15. The CRD (gold) forms a bundle of three alpha helices, while the TRXL domain (yellow) adopts a mixed α/β structure. U65 is exposed to solvent. (*C*) The helices of the CRD are held together by three disulfide bonds: C10-C42, C21-C43, and C24-C39. (*D*) The predicted structure creates a hydrophobic patch on part of the CRD (gold). Hydrophilic residues are shown in cyan. (*E*) The AlphaFold-multimer prediction of the UGGT1/SEP15 complex shows SEP15 interacting with UGGT1 via both domains and contacting UGGT1 SBR and TRXL4. The reactive U65 residue is proximal to the catalytic pocket of the GT domain.

C10-43, C21-C24, and C39-C43 (27). We are currently testing the AlphaFold2-predicted set of disulfide bridges experimentally. However, the predicted structure is characterized by high average pLDDT scores, >90 over residues 7 to 45, causing us to have high confidence in the prediction. In the predicted structure, one face of the CRD forms a concave surface featuring a hydrophobic patch that seems likely to be complementary to the patch on the putative SBD of UGGT (Fig. 3*D*). In addition, ConSurf analysis of SEP15 shows that the CRD surface is highly conserved (*SI Appendix*, Fig. S5), suggesting that it may be functionally relevant. We hypothesize that the hydrophobic surface on the CRD mediates the interaction with UGGT1.

The Predicted Structure of the UGGT1/SEP15 Complex Places the SEP15 Redox-Active Sec Residue Proximal to the UGGT1 Catalytic Site. To gain insight into the mechanistic role of SEP15 as a partner to UGGT, we predicted the structure of the human UGGT1/SEP15 complex using AlphaFold-multimer (Fig. 3*E*). Each monomer adopts a similar structure to that predicted for each protein in isolation. The structure confirms our hypothesis that the complementary hydrophobic patches in UGGT1 SBR and SEP15 CRD are situated at the interface between the two proteins. While the published biochemical analysis of the binding interaction between SEP15 and UGGT attributed the stabilization of the complex largely to the CRD, the predicted structure shows additional interactions between the UGGT1 TRXL4 and SEP15 TRXL domains. A continuous interface with a buried surface area of 1,860 Å^2 is formed in the complex. Importantly, roughly two-thirds of this contact area comes from the interaction between SEP15 CRD and UGGT1 SBR, and the remainder is contributed by the contacts between the SEP15 TRXL and UGGT1 TRXL4 domains This breakdown of the surface buried by each domain of SEP15 together with the published biochemical data (25) leads us to speculate that the CRD may act as an anchor, stably interacting with UGGT, while the TRXL interaction is more transient (see models below). ConSurf analysis (see above) showed that residues from both proteins within the observed interaction area are highly conserved.

The predicted CRD-SBR interaction is largely mediated by hydrophobic contacts as seen on the interface in the complex. UGGT residue F243 is inserted into a pocket on the CRD and makes contacts with SEP15 residues F15 and L27. The interface between SEP15 TRXL and UGGT TRXL4 is also largely composed of hydrophobic contacts. For instance, contacts are observed between SEP15 W118 and UGGT V278, and UGGT W279 contacts SEP15 F126.

We were excited to see that SEP15 is predicted to bind UGGT1 in an orientation that positions its TRXL domain in proximity to the catalytic pocket of the UGGT1 GT domain (Fig. 3*E*). The U65 residue of human SEP15 is exposed to the solvent and facing toward the large cleft running between the UGGT1 GT and TRXL2 domains. This binding mode would naturally position SEP15 to interact with a bound UGGT1 substrate.

Mutagenesis of UGGT1 to Test the AlphaFold Model of the UGGT1/SEP15 Complex. The AlphaFold2 model for the UGGT1/SEP15 complex predicts an interface between the CRD of SEP15 and a region in UGGT1 (here named "SBR"), which is consistent with prior hydrogen exchange mass spectrometry data (19). We tested the AlphaFold2 model for the complex by introducing mutations in the proposed SBR of UGGT1 that should disrupt the interaction with the CRD of SEP15. We identified residues within the predicted interface between SEP15 CRD and UGGT1 SBR that are most likely to contribute to the strength of the interface based on the solvent-accessible surface area (SASA) that is buried upon complex formation (*SI Appendix*, Table S1). UGGT1 F243 has the largest buried SASA when the complex is formed (91 Å^2) and is in the center of the interface. UGGT1 F244 has the second largest buried SASA when the complex forms (69 Å^2), and it is located on the periphery of the interface. UGGT1 L262 was the third most buried SASA upon complex formation (67 Å^2) and is positioned in the center of the interface, adjacent to F243. We hypothesized that individually mutating residues F243 and L262 to Lys would strongly perturb the interaction of UGGT1 with SEP15 according to the AlphaFold2 model.

To assess the impact of the designed UGGT1 mutations on the interaction with SEP15, we cotransfected HEK293 cells with HA-tagged SEP15 and FLAG-tagged UGGT1. Endogenous UGGT was detected with a polyclonal anti-UGGT antibody, but no UGGT was found upon coimmunoprecipitation using anti-FLAG antibody (Fig. 4*A*, lanes 1 and 2). SEP15 and UGGT1 were expressed

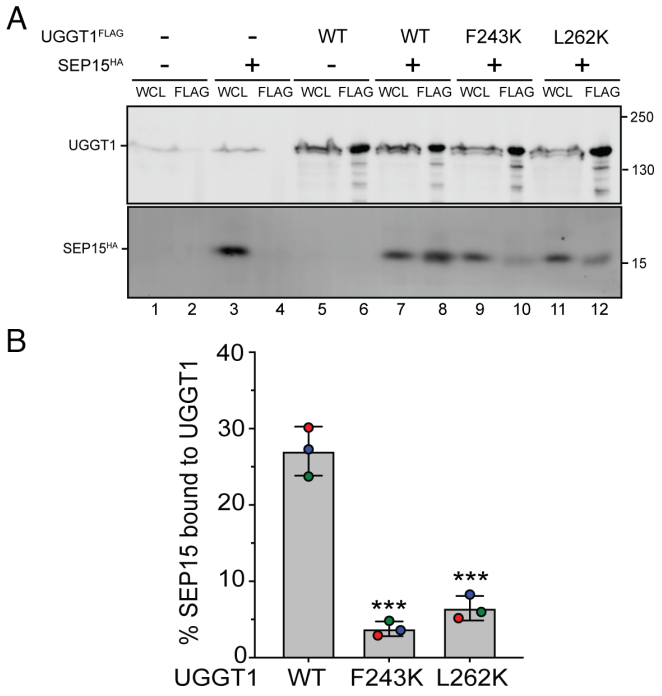

Fig. 4. AlphaFold-predicted point mutants disrupt UGGT1/SEP15 interaction. (*A*) SEP15, WT UGGT1, and UGGT1 mutants were exogenously expressed for 24 h into HEK293 cells. SEP15 contains an HA tag, whereas UGGT1 and the point mutants possess a 3xFLAG. Both tags are located on the C terminus of the protein. Cells were transfected and the following day were lysed to isolate their soluble cellular fractions. The resulting lysate was split between a whole cell lysate (WCL) fraction to identify the total amount of protein and a FLAG immunoprecipitation (IP) to isolate either free or SEP15-bound UGGT1. The resulting WCL and FLAG IPs were resolved using a 9% and 14% SDS-PAGE gel to probe for UGGT1 and SEP15, respectively, by western blot. UGGT1 was detected using an endogenous polyclonal antibody raised toward UGGT1, while SEP15 was detected using an HA polyclonal antibody. (*B*) Quantification of the percentage of SEP15 bound to UGGT1. The percent SEP15 bound to UGGT1 was determined by quantifying and normalizing the amount of SEP15 that co-IPs with UGGT1 (lanes 8, 10, and 12) and dividing it by the normalized amount of total SEP15 (lanes 7, 9, and 11) and multiplying by 100. *** indicates *P*-value < 0.001.

individually and showed no off-target binding (Fig. 4*A*, lanes 3 to 6). When plasmids encoding SEP15 and WT UGGT1 were cotransfected, both proteins were detected (Fig. 4*A*, lane 7). We confirmed SEP15 binding to wild-type (WT) UGGT1 by coimmunoprecipitation and found 27% of the expressed, detectable SEP15, in complex with UGGT1 (Fig. 4 *A*, *Bottom*, lane 8, Fig. 4*B*). Importantly, the two mutant UGGT constructs, F243K and L262K, expressed well and were detected by the UGGT1 antibody (Fig. 4 *A*, *Top*, lanes 9 and 11). Coimmunoprecipitation of the mutant UGGT1 with SEP15 showed that these mutations significantly disrupted complex formation (Fig. 4 *A*, *Bottom*, lanes 10 and 12). The L243K mutation resulted in only ~3.8% of SEP15 being bound to UGGT1, whereas the L262K mutant showed ~6.5% bound (Fig. 4*A*, lanes 9 and 11, Fig. 4*B*). These results provide experimental validation of the structural model for the UGGT1 complex with SEP15. Furthermore, this assay provides in cellulo evidence to support our model of the interaction of SEP15 with UGGT1 generated by AlphaFold2.

Quantitative Glycoproteomics Identifies Substrates with Altered UGGT Glucosylation in SELENOF Knockout Cells. One proposed function for UGGT-bound SEP15 is that SEP15 may aid in the selection of non-native clients for reglucosylation and reentry into the lectin chaperone cycle in a thiol-dependent manner. To investigate whether SEP15 modulates UGGT selectivity, a *SELENOF/ALG6*$^{-/-}$ double knockout was generated in HEK293 cells. Proteins synthesized in an *ALG6* knockout can only interact with lectin chaperones after UGGT recognition and modification, and not by the initial trimming step facilitated by GlsI and GlsII (Fig. 1, steps 2 and 5) as the glycans transferred to the nascent chain carry a $Man_9GlcNAc_2$ glycan. Proteins modified by UGGT can be isolated from cell lysates by affinity purification, using recombinantly produced CRT tagged with a glutathione-S-transferase tag (CRT), or a lectin-deficient CRT variant (CRT*) that lacks the ability to bind glycans. After affinity purification, CRT/CRT*-bound monoglucosylated proteins were labeled with tandem mass tags and analyzed by quantitative tandem mass spectrometry (*SI Appendix*, Fig. S6). This platform has been successfully used previously to identify substrates modified by UGGT in HEK293 cells and provides a method for identifying substrates affected by the absence of SEP15 (28, 29).

Comparison of the fold change in glucosylation between proteins expressed in the *SELENOF*$^{-/-}$*/ALG6*$^{-/-}$ cell line and the *ALG6*$^{-/-}$ parental cell line identified 26 proteins that were significantly affected by the deletion of SEP15, with a *P*-value < 0.05. Of these proteins, seven had a fold change resulting in a 50% increase or decrease in glucosylation by UGGT (Fig. 5). Analysis of these seven clients revealed that all were glycosylated (revealing interaction with UGGT) and contained a diverse range of cysteine residues (*SI Appendix*, Table S2). The size of the affected substrates was also highly variable, ranging from 288 to 2,039 amino acids, and they did not belong to a particular structural class (*SI Appendix*, Fig. S7). Three of the substrates were membrane proteins, while the remainder were soluble and secreted into the extracellular space. Taken together, these data suggest that SEP15 may not have a significant influence on the selectivity of UGGT, but rather serves some other function given the limited number of substrates affected by its absence compared to the established UGGT interactome (28). Additional work in more professional secretory cells or cells undergoing oxidative stress may reveal additional clients affected by SEP15 for efficient reglucosylation by UGGT.

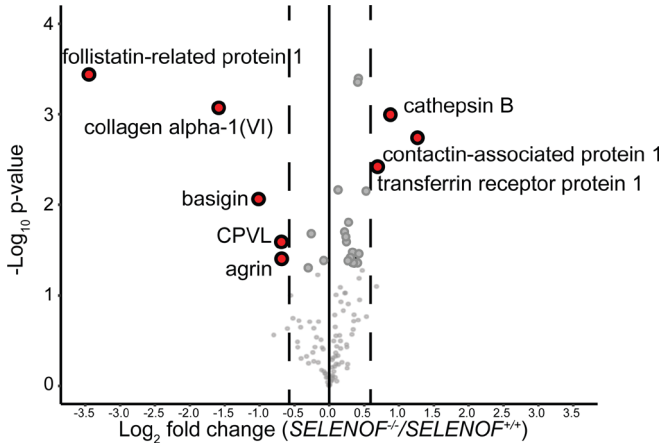

Fig. 5. Levels of UGGT glucosylation are altered in the absence of *SELENOF*. UGGT-modified substrates were isolated from *SELENOF*$^{+/+}$*/ALG6*$^{-/-}$ and *SELENOF*$^{-/-}$*/ALG6*$^{-/-}$ cells, and the changes in glucosylation were analyzed. Each point represents the change in glucosylation (log_2 fold change) between the *SELENOF*$^{-/-}$ divided by the *SELENOF*$^{+/+}$ cells in the *ALG6*$^{-/-}$ background and plotted against the $-log_{10}$ *P*-value. The dotted line indicates a 50% increase or decrease in levels of UGGT-mediated glucosylation. The large gray circles denote substrates in the *SELENOF*$^{-/-}$ that had a significant change in glucosylation (*P*-value < 0.05), compared to the parental cell line, but did not have fold change resulting in a 50% increase or decrease. Red circles indicate substrates with a fold change resulting in a 50% increase or decrease in glucosylation. Data are a result of three independent biological replicates. See *SI Appendix*, Table S2 for details on the labeled substrates.

Discussion

UGGT1 is a critical player in protein folding and maturation in the ER, acting as a gatekeeper to enable proteins to proceed to export from the ER or subjecting them to reglucosylation so that they reenter the lectin chaperone cycle for additional rounds of folding. A poorly understood partner of UGGT1, the selenoprotein SEP15, associates strongly with UGGT1. Intriguingly, while all SEP15 is UGGT1-associated, not all UGGT1 has a partner SEP15. This observation immediately raises the possibility that a subset of protein substrates relies on the collaboration between SEP15 and UGGT1. Prior to this work, structures were known for thermophilic yeast UGGTs, but these organisms lack SEP15. This motivated us to first obtain a structure for human UGGT to compare it to the yeast form and then to predict the structure of the complex with SEP15 to help deduce the role of this cochaperone. UGGT1 is a large (170 kDa) protein, and the UGGT1/SEP15 complex is even larger: 185 kDa. It is stunning that we now have the ability to predict structures for such large proteins and complexes, but in this case, the results are compelling.

The predicted structure of human UGGT1 revealed a domain arrangement similar to UGGT from the thermophilic yeast, but with an insertion that included a sequence formerly found to be protected from HDX upon complex formation with SEP15 (19). The presence of the sequence corresponding to this small domain only in UGGTs from organisms with SEP15s led to the hypothesis that this was the SEP15 binding site. This hypothesis was tested by applying AlphaFold2 to predict the structure of the UGGT1/SEP15 complex. Indeed, SEP15 was bound to the helix–loop–helix moiety present in the UGGT1 structure via its CRD, which had been shown to be responsible for most of the binding energy of SEP15 to UGGT1. Using a combination of mutagenesis and coimmunoprecipitations, we experimentally validated the interface between the two proteins predicted by AlphaFold2 (Fig. 4). This result has now enabled us to develop models for SEP15 mechanism of action. Most excitingly, the TRXL domain of SEP15, which carries the Sec or U residue in a C-G-U motif, is situated proximal to the GT domain of UGGT1. Moreover, this catalytic domain is adjacent to a large cleft that pierces the UGGT1 structure and is tantalizingly likely to be the site of substrate binding. As discussed, the proximity of the SEP15 reactive site to the GT catalytic site suggests that this complex acts on proteins with linkages between disulfide formation or mixing and assessment of foldedness, which triggers reglucosylation.

The AlphaFold2 predictions presented here enabled plausible models of UGGT1/SEP15 action to be developed. We hypothesize that SEP15 binds UGGT1 via a high-affinity interaction between the SEP15 CRD and UGGT1 SBR domains and a second, weaker, transient, interaction between the SEP15 TRXL and UGGT1 TRXL4 domains. The SEP15 TRXL would sample a conformational equilibrium between TRXL4-"docked" and "undocked" states (Fig. 6*A*). This conformational change could drive several aspects of function for UGGT/SEP15 complexes. First, SEP15 may aid UGGT in recruiting a substrate via formation of a selenyl-sulfide bond between U65 and a substrate Cys residue (Fig. 6*B*). Second, SEP15 may trap a glycan within the catalytic site of UGGT. In the predicted conformation, the SEP15 TRXL domain is partially blocking the glycan-binding pocket and would presumably hinder access in or out of this site. However, there is sufficient space that this configuration is likely compatible with a bound glycan. Third, the proximity between the SEP15 Sec and the UGGT GT catalytic pocket suggests that there is a limit on the distance between an N-glycosylation site and a disulfide bond that could be acted on by SEP15 within a substrate glycoprotein.

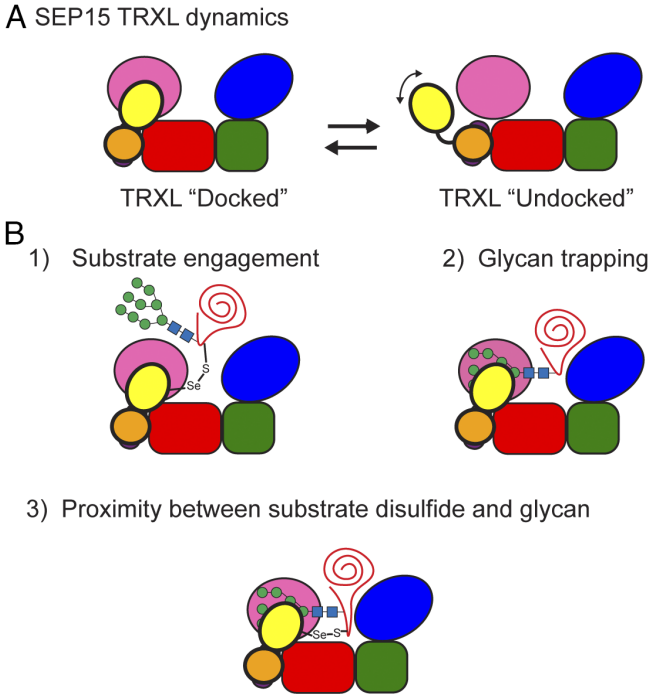

Fig. 6. Hypotheses for integrated UGGT1 and SEP15 action toward glycoprotein substrates. (*A*) Within UGGT1/SEP15 complexes, SEP15 may exist in a conformational equilibrium between two states. In the "docked" state, SEP15 TRXL (yellow) binds to UGGT1 TRXL4 (red), while in the "undocked" state, SEP15 TRXL is unbound. The SEP15 CRD (gold) maintains the interaction with UGGT1 in both cases. This conformational equilibrium can be exploited in the mechanism of action on substrates. (*B*) Possible modes of action for SEP15 within a UGGT1/SEP15 complex are proposed. Diagram 1) illustrates a model in which SEP15 may assist UGGT1 in engaging substrates via formation of a mixed selenyl-sulfide. Diagram 2) shows a model in which the SEP15 TRXL may trap a substrate glycan within the catalytic site of the UGGT GT domain. And in diagram 3), action of SEP15 may be most important for substrates in which an N-glycan and a disulfide bond occur at particular distances from one another, either through space or through sequence, taking advantage of the proximity of *the SEP*15 Sec residue and the catalytic site of UGGT GT (pink). Additionally, the TRXL2 (blue) and TRXL3 (green) domains are shown.

These three hypotheses are not mutually exclusive. It is plausible that they may act in combination to aid UGGT in glucosylating its client proteins. Future experiments are underway in our laboratory to explore UGGT/SEP15-substrate interactions.

In order to explore the implications of the possible models for the cooperative action of SEP15/UGGT1 on clients, we did an initial screen to identify proteins for which the level of reglucosylation was altered when SEP15 was absent (Fig. 5). Intriguingly, some substrates experienced increased reglucosylation, and others decreased when SEP15 was deleted. Decreased reglucosylation is consistent with the gatekeeping function that has been previously suggested for SEP15 (15). Species showing increased reglucosylation levels likely accumulate in non-native forms, suggesting that SEP15 may assist in proper maturation. Alternatively, SEP15 may facilitate degradation, and its deficiency could result in the accumulation of non-native species. Among those most impacted by the deletion of SEP15 were proteins of varying molecular weight (28 to 214 kDa), mixed structural class (α/β), and number of disulfides (*SI Appendix*, Fig. S8 and Table S2). Work is in progress to test models for the cooperation of SEP15 and UGGT1 on substrates, which will be informed by elucidating the proximity between disulfides and sites of glycosylation.

One of the more intriguing features of SEP15 is the presence of a Sec residue. This rare amino acid is only found in 25 human proteins, and its chemical properties make it highly reactive. In

SEP15, this residue is found within a C-G-U motif, which is truncated compared to the PDI class of oxidoreductases (30). The close spacing between the Cys and Sec residue likely creates a strained selenyl-sulfide bond and when combined with the inherent nucleophilicity of selenium would make this residue highly reactive. Within the context of our model, the Sec residue may facilitate rapid reactivity toward disulfide bonds within a client protein and assist rapid turnover of client glycoproteins by UGGT1/SEP15 complexes. While appealing, this speculation does not account for the observation that several SEP15 homologs (including *dm*Sep15) contain a Cys residue in place of the Sec. Future experiments will be necessary to solve the puzzle of the role of this reactive residue.

AlphaFold2 also predicts a helical domain topology for the SEP15 CRD. The six Cys residues within this domain are predicted to form three disulfide bonds that serve a structural role. These residues are closely spaced within the amino acid sequence, creating the deceptive appearance of reactive C-X-X-C motifs that are typical of PDIs. Instead, AlphaFold2 predicts that these residues form long-range disulfide bonds (Fig. 3*A*). A previous report of the disulfide pairing detected bonds between adjacent Cys residues within the CRD (27). Ultimately, this discrepancy awaits experimental determination of the pairing of SEP15 from a eukaryotic source.

AlphaFold2 has an impressive track record for predicting the structure of isolated proteins, with accuracy often rivaling that of experimental methods (20, 26). The development of the multimer extension to AlphaFold2 has also enabled accurate prediction of protein complexes (21). These tools have been incorporated into integrative structural studies of several large protein complexes including the cytoplasmic ring of the nuclear pore complex (31) and the OSTA-Sec61-TRAP complex (32). To the best of our knowledge, this report of the AlphaFold2 prediction of the 185 kDa UGGT1/SEP15 complex is one of the largest hetero-dimers predicted with this tool.

Ultimately, the advent of AlphaFold2 has enabled our prediction of a complex between a known major player in the ER protein maturation pathway, UGGT, and a mysterious cochaperone that has a selenocysteine residue in a functionally seductive location. The predicted model is highly compelling and allowed us to propose several functional hypotheses for this protein complex. We expect that these findings will drive further insights into ER protein quality control.

Materials and Methods

AlphaFold2 Predictions. Structural predictions were generated using AlphaFold v2.2.0 (20, 21). Human SEP15 was predicted using residues 32 to 165 from Uniprot entry O60613. As AlphaFold2 does not currently support selenocysteine residues, residue 96 was mutated to Cys. Human UGGT1 was predicted using residues 43 to 1,555 from Uniprot entry Q9NYU2. The UGGT1/SEP15 complex was predicted using the same residues in combination. All predictions were run on computer hardware made available through the NMRbox platform (33). All structural analyses and figures were produced using ChimeraX (23). The buried surface area was calculated using the "measure buriedarea" command, while the solvent-accessible surface area (SASA) was calculated using the "measure sasa" command. Both functions use a probe radius of 1.4 Å.

ConSurf. ConSurf analysis was performed using the ConSurf webserver (24) and using a custom multiple sequence alignment. An initial set of UGGT sequences was taken from a previous analysis of UGGT evolution (34) and the fungal sequences lacking a SEP15 counterpart were removed. The filtered set of sequences was aligned using Clustal Omega (35) and uploaded to the webserver for ConSurf analysis.

Mutagenesis. The gene encoding human UGGT1-FLAG was synthesized and cloned into a pcDNA3.1 expression vector (GeneArt Gene Synthesis, Thermo Fisher). UGGT1 mutants were generated by site-directed mutagenesis using overlapping oligonucleotide primers (IDT). The F243K mutant was generated using primers 5′-GATGAGGTGCAGGGCAAACTGTTCGGCAAGCTG-3′ and 5′-CAGCTTGCCGAACAGTTTGCCCTGCACCTCATC-3′, while the L262K mutation was generated with primers 5′-GGCCAGCTGAAAGAGGCCAGAAAGCACCTGGTG-3′and 5′-CACCAGGTGCTTTCTGGCCTCTTTCAGCTGGCC-3′.

Coimmunoprecipitation Assay. The protocol used is similar to that published previously (36), with modifications as described here. In a 6 cm plate, 1.75×10^6 HEK293 cells were plated and grown in DMEM (Sigma D5796) containing 10% fetal bovine serum (FBS) (Gibco 16000044) for 24 h. The next day, the cells were transfected with plasmids encoding SEP15 containing an HA tag, UGGT1 containing 3xFLAG, or cotransfected with plasmids encoding SEP15 and UGGT1, WT or either of the two-point mutants. Briefly, 4.8 μg of DNA was diluted in Opti-MemTM (Gibco 31985070) to a total volume of 80 μL. For the cotransfection, the DNA mixture was composed of 66% SEP15 and 33% UGGT1-encoding DNA. In a separate tube, 12 μL of PEI (Polyscience 24765), formulated at 1 mg/mL, was added to 68 μL of Opti-Mem and incubated at room temperature for 5 min. After incubation, the PEI-containing solution was added to the diluted DNA and incubated for an additional 20 min at 25 °C. The entire 160 μL of PEI:DNA mixture was added dropwise to each plate. The cells were returned to the incubator and incubated for 24 h at 37 °C in 5% CO_2.

Prior to lysis, the medium was removed, and the cells were washed with 1 mL of cold PBS and placed on ice. Then, 750 μL of lysis buffer (20 mM MES, 100 mM NaCl, 30 mM Tris pH 7.5, and 0.5% Triton X-100) containing both protease inhibitors (Thermo 1861278) and 20 mM N-ethylmaleimide was added to each plate and scraped to remove the attached cells. The lysate was removed and shaken vigorously for 10 min at 4 °C before centrifuging for 10 min at 20,817 × g at 4 °C. 20% (150 μL) of the lysate was used as the whole cell lysate (WCL) sample and 70% (525 μL) incubated with Protein-A-Sepharose® 4B resin (Invitrogen, 101042) coated with an α3xFLAG mouse monoclonal antibody (Sigma F1804). For the WCL, the lysate was mixed with 750 μL of cold acetone and incubated overnight at −20 °C. The next day, the samples were centrifuged for 10 min at 20,817 × g at 4 °C before the supernatant was removed and the pellets were allowed to air dry for an hour. For the 3xFLAG immunoprecipitation, 25 μL of the ProteinA resin was added to 74 μL of PBS and mixed with 1 μL of the α3xFLAG mouse monoclonal antibody. The solution was incubated for 1 h at 4 °C before being added to the immunoprecipitation sample. Once added, the solution was incubated overnight at 4 °C using an end-over-end spinner. The next day, the resin was pelleted at 950 × g for 5 min at 4 °C and washed twice with 500 μL of lysis buffer without protease inhibitor. Forty microliters of loading buffer (30 mM Tris-HCl pH 6.8, 9% SDS, 15% glycerol, and 0.05% bromophenol blue) containing 100 mM dithiothreitol (Sigma D9779) was added to both the WCL and immunoprecipitation samples, which were then treated for 10 min at 95 °C. Fifteen microliters of each sample was loaded in 9% and 14% SDS-PAGE gels to resolve UGGT1 and SEP15, respectively. The proteins were then transferred to a PVDF membrane (Millipore IPFL00010) and blotted using an αUGGT1 antibody (GeneTex GTX66459) and an αHA antibody (Cell Signaling Technologies C29F4) for SEP15-HA. A secondary, IRDye 680RD-conjugated αRabbit antibody was used for detection using chemiluminescence (LI-COR 926-68071).

The percentage of SEP15 bound to UGGT1 was calculated by quantifying and normalizing the signal from the WCL and immunoprecipitation lanes in the 14% gel using ImageQuant TL. The amount quantified in the 3xFLAG pulldown was then divided by the total amount of SEP15 in the WCL lanes and multiplied by 100. For quantification of the western blots, the SD is displayed and is representative of three independent biological replicates (n). Prism v9 was used for all quantifications and statistical analyses. Statistical significance was determined by using an unpaired *t* test with a minimal CI of 95%. Levels of significance denoted in the figure legends and data presented are the average of all biological replicates tested.

Cell Culture and SELENOF Knockout Generation. Detailed methods for cell culture and generation of the SELENOF knockout cells are given in *SI Appendix*.

Preparation of Lysate for Mass Spectrometry and Analysis of Samples by Mass Spectrometry. Detailed methods are provided in *SI Appendix*.

Data, Materials, and Software Availability. Structural coordinates data have been deposited in ModelArchive (ma-x205u (37), ma-qi383 (38), and ma-n3xv7 (39)).

ACKNOWLEDGMENTS. We thank Dr. Stephen Eyles for his expert assistance with mass spectrometry data collection and analysis. This work was supported by awards from the NIH (GM086874 to D.N.H. and GM118161 to L.M.G.) and a Chemistry–Biology Interface program training grant (T32GM008515 to K.P.G.). Mass spectrometry data were collected using the UMass Amherst Mass Spectrometry Core Facility (RRID:SCR_019063). This study made use of NMRbox: National Center for Biomolecular NMR Data Processing and Analysis, a Biomedical Technology Research Resource (BTRR), which is supported by NIH grant P41GM111135 (NIGMS). Molecular graphics and analyses were performed with UCSF ChimeraX, developed by the Resource for Biocomputing, Visualization, and Informatics at UCSF, with support from NIH GM129325 and the Office of Cyber Infrastructure and Computational Biology, NIAD.

1. A. Kanapin *et al.*, Mouse proteome analysis. *Genome Res.* **13**, 1335–1344 (2003).
2. R. Apweiler, H. Hermjakob, N. Sharon, On the frequency of protein glycosylation, as deduced from analysis of the SWISS-PROT database. *Biochim. et Biophys. Acta Gen. Subj.* **1473**, 4–8 (1999).
3. C. Hammond, I. Braakman, A. Helenius, Role of N-linked oligosaccharide recognition, glucose trimming, and calnexin in glycoprotein folding and quality control. *Proc. Natl. Acad. Sci. U.S.A.* **91**, 913–917 (1994).
4. B. M. Adams, M. E. Oster, D. N. Hebert, Protein quality control in the endoplasmic reticulum. *Protein J.* **38**, 317–329 (2019).
5. D. F. Zielinska, F. Gnad, J. R. Wiśniewski, M. Mann, Precision mapping of an in vivo N-glycoproteome reveals rigid topological and sequence constraints. *Cell* **141**, 897–907 (2010).
6. G. Kozlov, K. Gehring, Calnexin cycle–Structural features of the ER chaperone system. *FEBS J.* **287**, 4322–4340 (2020).
7. J. J. Caramelo, O. A. Castro, L. G. Alonso, G. de Prat-Gay, A. J. Parodi, UDP-Glc:glycoprotein glucosyltransferase recognizes structured and solvent accessible hydrophobic patches in molten globule-like folding intermediates. *Proc. Natl. Acad. Sci. U.S.A.* **100**, 86–91 (2003).
8. C. Ritter, K. Quirin, M. Kowarik, A. Helenius, Minor folding defects trigger local modification of glycoproteins by the ER folding sensor GT. *EMBO J.* **24**, 1730–1738 (2005).
9. C. Ritter, A. Helenius, Recognition of local glycoprotein misfolding by the ER folding sensor UDP-glucose:glycoprotein glucosyltransferase. *Nat. Struct. Mol. Biol.* **7**, 278–280 (2000).
10. C. P. Modenutti *et al.*, Clamping, bending, and twisting inter-domain motions in the misfold-recognizing portion of UDP-glucose: Glycoprotein glucosyltransferase. *Structure* **29**, 357–370.e9 (2021).
11. P. Roversi *et al.*, Interdomain conformational flexibility underpins the activity of UGGT, the eukaryotic glycoprotein secretion checkpoint. *Proc. Natl. Acad. Sci. U.S.A.* **114**, 8544–8549 (2017).
12. K. V. Korotkov, E. Kumaraswamy, Y. Zhou, D. L. Hatfield, V. N. Gladyshev, Association between the 15-kDa Selenoprotein and UDP-glucose:glycoprotein glucosyltransferase in the endoplasmic reticulum of mammalian cells. *J. Biol. Chem.* **276**, 15330–15336 (2001).
13. V. M. Labunskyy, M.-H. Yoo, D. L. Hatfield, V. N. Gladyshev, Sep15, a thioredoxin-like selenoprotein, is involved in the unfolded protein response and differentially regulated by adaptive and acute ER stresses. *Biochemistry* **48**, 8458–8465 (2009).
14. M. V. Kasaikina *et al.*, Roles of the 15-kDa selenoprotein (Sep15) in redox homeostasis and cataract development revealed by the analysis of Sep 15 knockout mice. *J. Biol. Chem.* **286**, 33203–33212 (2011).
15. S. H. Yim *et al.*, Role of Selenof as a gatekeeper of secreted disulfide-rich glycoproteins. *Cell Rep.* **23**, 1387–1398 (2018).
16. V. M. Labunskyy, D. L. Hatfield, V. N. Gladyshev, Selenoproteins: Molecular pathways and physiological Roles. *Physiol. Rev.* **94**, 739–777 (2014).
17. E. S. J. Arnér, Selenoproteins–What unique properties can arise with selenocysteine in place of cysteine? *Exp. Cell Res.* **316**, 1296–1303 (2010).
18. A. D. Ferguson *et al.*, NMR structures of the selenoproteins Sep15 and SelM reveal redox activity of a new thioredoxin-like family. *J. Biol. Chem.* **281**, 3536–3543 (2006).
19. D. Calles-Garcia *et al.*, Single-particle electron microscopy structure of UDP-glucose:glycoprotein glucosyltransferase suggests a selectivity mechanism for misfolded proteins. *J. Biol. Chem.* **292**, 11499–11507 (2017).
20. J. Jumper *et al.*, Highly accurate protein structure prediction with AlphaFold. *Nature* **596**, 583–589 (2021).
21. R. Evans *et al.*, Protein complex prediction with AlphaFold-Multimer. biorxiv [Preprint] (2022). https://www.biorxiv.org/content/10.1101/2021.10.04.463034v2.abstract (Accessed 15 December 2023).
22. T. Satoh *et al.*, Visualisation of a flexible modular structure of the ER folding-sensor enzyme UGGT. *Sci. Rep.* **7**, 12142 (2017).
23. E. F. Pettersen *et al.*, UCSF ChimeraX: Structure visualization for researchers, educators, and developers. *Protein Sci.* **30**, 70–82 (2021).
24. B. Yariv *et al.*, Using evolutionary data to make sense of macromolecules with a "face-lifted" ConSurf. *Protein Sci.* **32**, e4582 (2023).
25. V. M. Labunskyy *et al.*, A novel cysteine-rich domain of Sep15 mediates the Interaction with UDP-glucose:glycoprotein glucosyltransferase. *J. Biol. Chem.* **280**, 37839–37845 (2005).
26. K. Tunyasuvunakool *et al.*, Highly accurate protein structure prediction for the human proteome. *Nature* **596**, 590–596 (2021).
27. P. Liao, C. He, Chemical synthesis of the Sec-To-Cys homologue of human selenoprotein F and elucidation of its disulfide-pairing mode. *Front. Chem.* **9**, 735149 (2021).
28. B. M. Adams, N. P. Canniff, K. P. Guay, I. S. B. Larsen, D. N. Hebert, Quantitative glycoproteomics reveals cellular substrate selectivity of the ER protein quality control sensors UGGT1 and UGGT2. *Elife* **9**, e63997 (2020).
29. K. P. Guay *et al.*, ER chaperones use a protein folding and quality control glyco-code. *Mol. Cell* **83**, 4524–4537.e5 (2023), 10.1016/j.molcel.2023.11.006.
30. G. Kozlov, P. Määttänen, D. Y. Thomas, K. Gehring, A structural overview of the PDI family of proteins. *FEBS J.* **277**, 3924–3936 (2010).
31. P. Fontana *et al.*, Structure of cytoplasmic ring of nuclear pore complex by integrative cryo-EM and AlphaFold. *Science* **376**, eabm9326 (2022).
32. M. Gemmer *et al.*, Visualization of translation and protein biogenesis at the ER membrane. *Nature* **614**, 160–167 (2023).
33. M. W. Maciejewski *et al.*, NMRbox: A resource for biomolecular NMR computation. *Biophys. J.* **112**, 1529–1534 (2017).
34. L. I. Buzzi, S. H. Simonetta, A. J. Parodi, O. A. Castro, The two caenorhabditis elegans UDP-glucose:glycoprotein glucosyltransferase homologues have distinct biological functions. *PLoS One* **6**, e27025 (2011).
35. F. Sievers *et al.*, Fast, scalable generation of high-quality protein multiple sequence alignments using clustal omega. *Mol. Sys. Biol.* **7**, 539 (2011).
36. G. Tax *et al.*, Rescue of secretion of a rare-disease associated misfolded mutant glycoprotein in *UGGT1*knock-out mammalian cells. *Traffic* 25, e12927 (2024).
37. R. V. Williams, "Human UGGT1/SEP15 heterodimer." ModelArchive. https://www.modelarchive.org/doi/10.5452/ma-x205u. Deposited 5 October 2023.
38. R. V. Williams, "Human SEP15 U65C." ModelArchive. https://www.modelarchive.org/doi/10.5452/ma-qi383. Deposited 5 October 2023.
39. R. V. Williams, "Human UGGT1." ModelArchive. https://www.modelarchive.org/doi/10.5452/ma-n3xv7. Deposited 5 October 2023.